Phys. Rev. A 2, 107 (1970); 3, 509 (1971).
[3]P. S. Ganas and A. E. S. Green, Phys. Rev. A 4, 182 (1971).
[4]T. Sawada, J. E. Purcell, and A. E. S. Green, Phys. Rev. A 4, 193 (1971).
[5]R. A. Berg and A. E. S. Green, Advan. Quantum Chem. (to be published).
[6]C. E. Moore, *Atomic Energy Levels*, Natl. Bur. Std. (U.S.) Circ. No. 467 (U. S. GPO, Washington, D.C., 1958), Vol. I.
[7]A. Messiah, *Quantum Mechanics*, Vol. II (North-Holland, Amsterdam, 1958), Appendix C.
[8]A. R. Edmonds, *Angular Momentum in Quantum Mechanics* (Princeton U. P., Princeton, N. J., 1957).
[9]B. W. Shore and D. H. Menzel, *Principles of Atomic Spectra* (Wiley, New York, 1968).
[10]Y. K. Kim, M. Inokuti, G. E. Chamberlain, and S. R. Mielczarek, Phys. Rev. Letters 21, 1146 (1968).
[11]E. J. McGuire, Sandia Labs. Res. Rept. No. SC-RR-70-406, 1971 (unpublished).
[12]A. E. S. Green and S. K. Dutta, J. Geophys. Res. 72, 3933 (1967).
[13]E. J. Stone and E. C. Zipf, Phys. Rev. A 4, 610 (1971).
[14]U. Fano and J. W. Cooper, Phys. Rev. 137, A1364 (1965).
[15]P. S. Kelly, J. Quant. Spectry. Radiative Transfer 4, 117 (1964).
[16]A. B. Prag, C. E. Fairchild, and L. C. Clarn, Phys. Rev. 137, A1358 (1965).
[17]F. A. Morse and F. Kaufman, J. Chem. Phys. 42, 1785 (1965).
[18]D. A. Parkes, L. F. Keyser, and F. Kaufman, Astrophys. J. 149, 217 (1967).
[19]G. Boldt and F. Labuhn, Z. Naturforsch. A22, 1613 (1967).
[20]C. Lin, D. A. Parkes, and F. Kaufman, J. Chem. Phys. 53, 3896 (1970).
[21]B. D. Savage and G. M. Lawrence, Astrophys. J. 146, 940 (1966).
[22]J. E. Hesser, J. Chem. Phys. 48, 2518 (1968).
[23]G. M. Lawrence and M. George, Phys. Rev. 175, 40 (1968).
[24]W. L. Fite and R. T. Brackmann, Phys. Rev. 113, 815 (1959).
[25]A. Boksenberg, thesis (University of London, 1961) (unpublished).
[26]M. J. Seaton, Phys. Rev. 113, 814 (1959).
[27]L. J. Kieffer, Compilation of Low Energy Electron Collision Cross Section Data, Part I, JILA Information Center Rept. No. 6, University of Colorado, 1969 (unpublished).

PHYSICAL REVIEW A VOLUME 6, NUMBER 6 DECEMBER 1972

Dissociative Excitation of Molecular Hydrogen by Electron Impact*

Martin Misakian† and Jens C. Zorn
Randall Laboratory of Physics, The University of Michigan, Ann Arbor, Michigan 48104
(Received 23 August 1971; revised manuscript received 26 June 1972)

Dissociative excitation of molecular hydrogen can proceed via the process $H_2+e\rightarrow H(2s)+H+e$ and yield metastable H(2s) atoms that have kinetic energies near 0.3 eV ("slow") or near 4 eV ("fast"). The dissociation process has been studied using a pulsed electron gun with an energy resolution of ± 0.3 eV and using a metastable atom detector capable of viewing H(2s) atoms with an angular resolution of 1° over a range 60°–120° with respect to the electron-beam direction. The measurement of the angular intensity distribution gives information about the final states that are involved in the dissociation process. (i) For slow H(2s) atoms, the electron energy threshold for production of the least energetic of the slow metastable atoms is 14.6 ± 0.3 eV. The excitation function and the angular distribution of the slow H(2s) atoms suggest that the $B'\,^1\Sigma_u^+$, $e\,^3\Sigma_u^+$, $D\,^1\Pi_u^+$, and $d\,^3\Pi_u^+$ excited states are involved in the formation of these metastable fragments. (ii) For fast H(2s) atoms, the electron energy threshold for production of the least energetic of the fast H(2s) atoms is near 29 eV. The angular distribution data would indicate that these atoms arise from a Π_u state; the form of the excitation function indicates that the parent state has a multiplicity of 1. The change in energy distribution of the fast H(2s) atoms, measured as a function of electron-gun voltage, supports the view that the $^1\Pi_u$ state is a previously unreported doubly excited state that has an asymptotic energy of 24.9 eV.

I. INTRODUCTION

Recently Leventhal, Robiscoe, and Lea[1] employed a time-of-flight (TOF) technique to measure the energy distributions of metastable H(2s) atom fragments that were produced via the process

$$H_2+e\rightarrow H(2s)+H+e\ .$$

H(2s) atoms were produced by pulsing a simple triode electron gun in an H_2 atmosphere. The metastable atoms moved translationally with kinetic energy released during the dissociation process and after some collimation entered a "quench" region 10 cm away. A strong electric field was applied in this region which mixed the $2S_{1/2}$ and $2P_{1/2}$ states causing a decay to the ground state.

The Lyman-α decay photon was then detected with a photomultiplier tube. The time interval between the electron-gun pulse and the detection of a photon was measured to yield a TOF distribution of the H(2s) atoms produced in the dissociation process.

While the work done by Leventhal *et al.* was reported as preliminary, several interesting features were observed. The dissociative excitation process yielded atomic fragments in two distinct kinetic energy groups that were designated as "slow" (energies near 0.3 eV) and "fast" (energies near 4.5 eV). The slow H(2s) atoms were believed to arise from transitions to singly excited states of H_2 just above the H(1s)+H(2s) separated-atom limit. The fast H(2s) atoms were thought to come from transitions to previously undetected doubly excited repulsive states. Rough measurements of the threshold energies required to produce the fast and slow transitions were also made.

Matters which required further study included (a) the identification of the final states involved in the dissociative excitation process, (b) an unexplained cutoff at low energies in the slow H(2s) energy distribution, (c) a marked angular dependence of the fast H(2s) energy distribution for angles near 90° with respect to the electron-beam direction, and (d) a more precise determination of the threshold energies.

Since the work of Leventhal *et al.*, three experimental studies have touched upon the present problem. Clampitt and Newton[2] examined the TOF spectrum of the slow H(2s) atoms using a crossed-beams arrangement. Their results showed no cutoff at very low energies in the energy distribution of slow H(2s) atoms and thus contrasted with the results of Leventhal *et al.* More recently Czarnik and Fairchild,[3] examining the TOF spectra of slow H(2s) atoms (using cooled target molecules), concluded that the H(2s) atoms arose mainly from predissociation of the $D\,^1\Pi_u$, $8p\sigma\,^1\Sigma_u^+$ ($v=5$), $8p\sigma\,^3\Sigma_u^+$ ($v=4$), and $9p\sigma\,^1\Sigma_u^+$ ($v=5$) states. In addition, a study has been done and briefly reported[4] by the present authors; the detailed description and final conclusions of that study are given here.

The present experiment employed a pulsed electron beam to excite a diffuse gas of H_2 molecules. The energy resolution of the electron gun permitted careful measurements of the thresholds for the production of slow and fast H(2s) atoms. Moreover, the experiment was done in a vacuum system that facilitated a systematic study of the angular distribution of the fragments in the dissociative excitation process. The results permit the identification of the several excited states that are involved in the production of the H(2s) fragments. What appears to be of particular significance is the identification of a previously unreported excited state in molecular hydrogen.

II. DISSOCIATIVE EXCITATION PROCESS

A. Direct Dissociation

Figure 1 is a schematic representation of the dissociative excitation process in molecular hydrogen. An electron of controlled energy collides with the H_2 molecule in the $X\,^1\Sigma_g^+$ ground state and excites the molecule "vertically" in the Franck-Condon region. If the transition is to a point above the asymptotic limit of the final-state potential, the constituent H atoms can come apart with kinetic energy of the order of several eV. The total energy released during the dissociation process is given by the difference between the excitation energy and the asymptotic limit.

The transition matrix element for the dissociative excitation process is

$$T = C\int e^{i\vec{k}\cdot\vec{r}}\Psi_I P\Psi_F^*\Phi^*\, dR\, d\tau_e\,, \tag{1}$$

where $\hbar\vec{k}$ is the momentum of the incident electron, Ψ_I is the ground-state molecular wave function, Ψ_F is the final-state wave function, Φ is the wave function of the scattered electron (possibly exchanged), $d\tau_e$ is the volume element of the electronic coordinates, R is the internuclear separation, and C is a constant. The perturbation P is taken to be just a sum of Coulomb interaction terms between the incident electron and molecule.

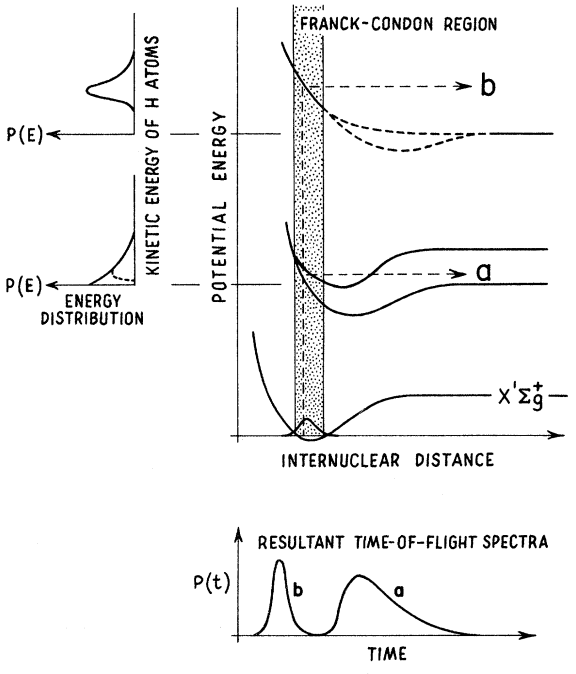

FIG. 1. Schematic of dissociative excitation process leading to slow (path a) and fast (path b) metastable H(2s) atoms. Predissociation may occur when the potential curves of two states approach one another.

Ab initio calculations of T from Eq. (1) would be quite difficult, but much can be learned about the transition matrix element by considering the kinetic energy distribution and the angular distribution of the dissociation fragments.

1. Kinetic Energy Distribution

The transition matrix element calculation can be greatly simplified by an application of the Franck-Condon principle. Because of the relatively large masses of the nuclei in the molecule, the assumption is made that their momenta will not be directly affected by electronic transitions.[5] This separability of nuclear and electronic motions permits one to write the molecular wave functions as a product of electronic and nuclear wave functions. Using this approximation, Harriman[6] has shown that the probability for dissociative excitation of H_2 from electron collision is

$$|T|^2 \propto [\int U(R)V(R)\,dR]^2 , \tag{2}$$

where $U(R)$ is the lowest vibrational wave function in the $X\,^1\Sigma_g^+$ state, $V(R)$ is the vibrational wave function of an excited state with energy above the dissociative limit, and R is the internuclear distance.

A further simplication can be had by making another approximation first used by Winans and Stueckelburg.[7] The vibrational wave function of the final state is replaced by a δ function $\delta(R-R_0)$, which is nonzero at the classical turning point of the potential curve. The results obtained with this approximation differ little from those found by using accurate vibrational wave functions.[8,9] The probability for a transition to occur when the internuclear distance is between R_0 and R_0+dR_0 then becomes proportional to

$$|U(R_0)|^2 dR_0 . \tag{3}$$

This result has a very graphic interpretation and two examples (a and b) are shown in Fig. 1. The energy distributions of the dissociated fragments can be regarded as reflections of $|U(R)|^2$ through the final-state potential curves onto an energy axis. When the Franck-Condon region encloses a portion of the excited potential curve containing the asymptotic energy (transition a), slow H atoms should be produced with high probability. When the region of intersection is well above the asymptotic energy (transition b) only fast H atoms are produced. The slow H(2s) atoms discussed in Sec. V are believed to arise in part from transitions of type a while the fast H(2s) atoms discussed in Sec. VI arise from transitions of type b.

An important consideration is the influence of thermal motion of the parent molecules on the energy distribution of the dissociated atoms. If the atom acquires a velocity V_0 from the kinetics of the dissociation process, and if the molecules (mass M) in the target gas have a Maxwellian velocity distribution characterized by the temperature T, then the atom fragments will have a velocity distribution given by[10]

$$\frac{dN}{N} = \left(\frac{2M}{\pi kT}\right)^{1/2} \frac{V}{V_0} \exp\left(\frac{-M(V_0^2+V^2)}{2kT}\right) \times \sinh\left(\frac{MV_0V}{kT}\right) dV . \tag{4}$$

Here dN/N is the fraction of the dissociated atoms having a lab speed between V and $V+dV$. The effect of the molecular thermal motion is to broaden the energy distributions mentioned above.

2. Angular Distribution of Fragments

Dunn[11] has pointed out that the symmetry axis for the electron-molecule system is the electron momentum exchange vector $\vec{K}$, and that dissociative excitation processes may show a marked dependence on the molecular orientation with respect to this axis. At threshold energies for dissociation, the symmetry axis coincides with the electron-beam direction $\vec{k}$. Above the threshold energy, the most probable direction of $\vec{K}$ will be a function of the electron energy. These two cases are discussed briefly.

Behavior at threshold. If the electron energy is near the threshold for dissociation, the outgoing electrons will have an s-wave distribution; this high degree of symmetry in the wave function of the scattered electron makes it possible to use the direction of the incoming electron beam as an axis of symmetry in a discussion of the angular distribution of the outgoing atoms in the dissociation process. Dunn[11] noted that because the perturbation P is a scalar sum of Coulomb terms, the initial- and final-state wave functions would have to transform according to the same irreducible representation in order that the matrix element not vanish. Expressed more simply, the wave functions must transform in the same way if operated on by operators which preserve the physical symmetries present during the collision process. The consequences of this observation led Dunn to construct a table of matrix-element behavior for certain molecular orientations with respect to the direction of the electron beam. A portion of the table which applies for dissociative excitation in H_2 with electron energies *at threshold* is shown in Fig. 2. The matrix-element behavior for perpendicular molecular orientations with respect to the electron-beam direction is shown to the left of the vertical bars and the behavior for parallel orientations is to the right. The symbol × indicates a nonzero value and o a zero value.

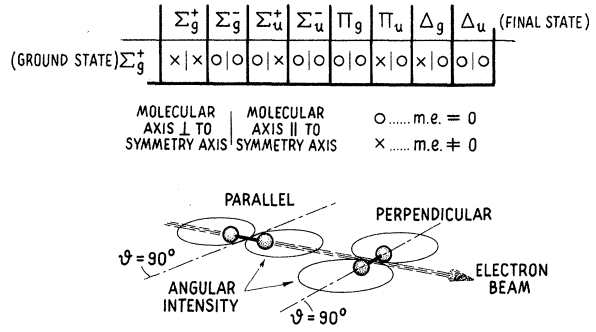

FIG. 2. Behavior of transition matrix element between pairs of electronic states with electron energies at threshold (after Ref. 11). Entries to the left of the vertical bars indicate matrix element behavior for perpendicular molecular orientations and entries to the right are for parallel orientations. Qualitative angular distributions of the atom fragments are also shown assuming dissociation occurs in a time which is short compared to the period of rotation.

Since direct dissociation occurs in a time which is short compared to the period for molecular rotation,[12] the H-atom trajectory will indicate to good approximation the molecule's orientation in space. The angular distribution of dissociated atoms can thus reveal the molecule's orientation at the time of dissociation. Fragment angular distributions for "parallel" and "perpendicular" transitions are qualitatively sketched in Fig. 2. A parallel transition leads to possible maxima in the angular distribution at $\theta = 0°$ and $180°$ while a perpendicular transition leads to possible maxima at $90°$ and $270°$ (here θ is the angle between the electron beam and the line of observation). With Dunn's table, therefore, a measurement of the fragment angular distribution can be of considerable help in the assignment of the excited state(s).

Behavior above threshold. For electron energies well above threshold, the most probable direction of $\vec{K}$ no longer coincides with the electron-beam direction. At higher electron energies, however, the relation $K \ll 1/a_0$ is satisfied (a_0 is the Bohr radius) and the transition probability can be expanded[13] in powers of K. The leading and dominant term in this expansion is proportional to $|\vec{K}\cdot\langle\vec{M}\rangle|^2$, where $\langle\vec{M}\rangle$ is the dipole matrix element and K is the momentum-change vector $\vec{k}-\vec{k}'$ of the scattered electron. Zare and Herschbach[12] have explained in detail how this probability can be transformed into lab-system coordinates. The angular distributions above threshold are given by the following "practical approximations":

$$I(\theta) = A(\cos^2\beta\cos^2\theta + \tfrac{1}{2}\sin^2\beta\sin^2\theta) \qquad (5)$$

for $\Delta\Lambda = 0$ ($\Sigma \leftrightarrow \Sigma$, $\Pi \leftrightarrow \Pi$, etc.), and

$$I(\theta) = A'[2\cos^2\beta\sin^2\theta + \sin^2\beta(1+\cos^2\theta)] \qquad (6)$$

for $\Delta\Lambda \neq 0$ ($\Sigma \leftrightarrow \Pi$, $\Pi \leftrightarrow \Delta$, etc.).

Here A and A' depend on the electron energy (but not θ); β is the most probable angle between $\vec{K}$ and $\vec{k}$ and is a function of fragment atom and electron energies; θ is the angle between the electron-beam direction and the line along which fragments are observed; Λ is the component of the orbital electronic angular momentum along the internuclear axis. For small values of β, $I(\theta)$ is weighted more as a $\cos^2\theta$ distribution for $\Delta\Lambda = 0$ and as a $\sin^2\theta$ distribution for $\Delta\Lambda \neq 0$. This is compatible with the more qualitative results at threshold shown in Fig. 2, although the $|\vec{K}\cdot\langle\vec{M}\rangle|^2$ term is not dominant at threshold. As the electron energy is increased, the angle β increases and $I(\theta)$ becomes increasingly isotropic. At $\beta = 54.7°$, $I(\theta)$ is isotropic for both classes of electronic transitions.

Sasaki and Nakao[14] appear to be the first to have experimentally observed an anisotropy in the angular distribution of fragments from H_2 following dissociation by electron impact. More recently Dunn and Kieffer[15] and Van Brunt and Kieffer[16] have shown the approximate validity of the foregoing analyses for dissociative ionization of H_2. Zare[17] has also calculated in detail the angular distribution of H^+ from dissociation of H_2^+. Theoretical predictions for this process, which should be similar to dissociative ionization, bear a striking and reassuring resemblance to the data of Dunn and Kieffer. Indeed, the angular distribution of H^+ from dissociative ionization of H_2 (a $\Delta\Lambda = 0$ type transition) near threshold cannot be accurately described by Eq. (5). However, an excellent theoretical fit to their angular distribution data can be made[16,17] (aside from an unexplained isotropic component) using the results of Zare's detailed calculation for the dissociation of H_2^+.

B. Predissociation

The electron-molecule collision may excite the molecule to a bound electronic state that merges energetically with the repulsive portion of a lower-lying state. Mixing of the two states can occur in the region of near energy coincidence through heterogeneous and homogeneous perturbations.[18] The calculation of the coupling matrix elements between the states leads to Franck-Condon overlap integrals whose values are normally large only on or near points of intersection of the molecular potentials. The radiationless transition induced by the mixing leads to dissociation. This is the process of predissociation.

Because predissociation is considerably slower than direct dissociation,[19,20] the molecule may undergo several rotations before breaking apart.

Yet the angular distribution of fragments arising from predissociation retains some of the anisotropy inherent in the original excitation. In photodissociation, for example, Jonah has shown[21] that a perpendicular transition followed by predissociation in characteristic time τ gives rise to an angular distribution

$$I(\theta)=\frac{(\sin^2\theta/\tau\omega)+3\tau\omega-\tau\omega\cos^2\theta}{8\tau\omega+2/\tau\omega},$$

where ω is the rate of molecular rotation. Jonah's results can be used to describe electron-impact-induced predissociation if the momentum transfer vector $\vec{K}$ is identified with his electric field vector $\vec{E}$.

The time required for predissociation in H_2 can be estimated from the width of lines seen in optical absorption as transitions are made to the predissociating levels. Thus the rotation time for the $J=1$ state of H_2 ($1/\omega \simeq 2\times10^{-14}$ sec) is far shorter than the $\tau \simeq 10^{-11}$-sec lifetime implied by the ~1-cm^{-1} linewidths that are typical. Under these conditions $\omega\tau \gg 1$ and Jonah's expression predicts the angular distribution of fragments from predissociation following a perpendicular transition to be proportional to $3-\cos^2\theta$.

C. Kinematic Distortion of Angular Distributions

As a final observation, it is noted that the above theory has been developed under the assumption that the collision process does not significantly affect the trajectory of the molecular center-of-mass motion. This is not the case[16,22] as will be seen shortly; in fact the experimental angular distributions clearly show the effect of the collision kinematics.

III. APPARATUS

A. Vacuum System

The experiment was carried out in a brass vacuum system (Fig. 3) that consisted of (i) a stationary source chamber containing the electron gun and the gas cell, and (ii) a detector chamber that could be rotated about the center of the source chamber. Each chamber was pumped separately with a 700-liter/sec diffusion pump that employed a silicone pump oil (DC 705). Above each pump was a baffle that was usually refrigerated to about -10 °C during pump-down of the system, and above each baffle was a liquid-nitrogen trap that was always filled when measurements were being made. The system pressures were monitored by RCA type 1949 ionization gauges that had been indirectly calibrated with a McLeod gauge. The base pressure of the vacuum system, without gas being fed to the source chamber, was on the order of 2×10^{-7} Torr.

B. Electron-Gun Construction

The electron gun used in this experiment is similar to the one developed by McFarland.[23] Its general construction can be seen in Fig. 3; a detailed description is given in Ref. 29. Indirectly heated Philips cathodes (Philips Metalonics, Mt. Vernon, New York) with type-A and -B impregnants were used as the electron source. Because metal vapors which alloy with tungsten (iron and nickel, for example) will poison the cathode, the accelerator grid which was closest to the cathode was made of molybdenum. The remaining grids, made of No. 316 stainless steel, were 0.025×1.25 cm in diameter with 0.20-cm apertures for the electron beam. The space between the fifth and sixth grids was enclosed by a 1.25-cm-long$\times1.10$-cm-diam cylinder (No. 316 stainless steel) and served as the interaction region.

Gas entered the interaction region from a small tube, and a deflection plate was mounted just at the tube opening to ensure that the target molecules in the interaction region would be in the form of a diffuse gas. The front of the interaction region had a 0.05×1.25-cm horizontal slit that served as the exit for the observed metastable atoms. The temperature of the interaction region, as measured with a thermocouple, usually exceeded 100 °C because of heat transferred from the cathode.

C. Electron-Gun Energy Resolution and Calibration

An estimate of the electron energy spread was made by examining the excitation function for pro-

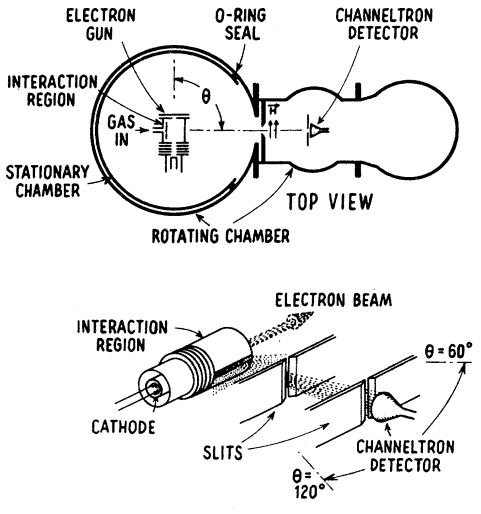

FIG. 3. Schematic of vacuum chamber and interaction region. The moveable detector chamber could be rotated about the chamber enclosing the electron gun from $60°<\theta<120°$. A localized magnetic field behind the first slit removed charged particles from the beam.

ducing metastable helium atoms. A graph of metastable atoms produced versus electron voltage (uncalibrated) is shown in Fig. 4. The metastable helium atoms were detected with a Channeltron (discussed below) and were counted for several 10-sec intervals with a frequency counter. Fox *et al.*[24] have shown that the electron energy spread is nearly twice the width of the tail at threshold. Using the electron gun described above, the tail was found to be about 0.3 eV wide. Moreover, the triplet helium $2\,^3S$ and singlet $2\,^1S$ metastable states were also partially resolved. Because the singlet and triplet energy levels are only 0.8 eV apart, this resolving of the two states lends further support to the estimate of an 0.6-eV electron energy spread. Thus there is an uncertainty of about ±0.3 eV in the specification of electron energies in this experiment.

The electron-gun voltage scale was calibrated before every run by measuring the threshold electron-gun voltage for producing triplet $2\,^3S$ helium atoms and comparing it with the known value of 19.82 eV. This procedure was checked on occasion by repeating the process using argon gas (11.55-eV threshold energy). The difference between the threshold electron energy and the experimental (voltmeter) value was found to be nearly the same for both gases.

D. Detector

In this experiment, metastable atoms and molecules were detected with a windowless, continuous-channel electron multiplier ("Channeltron" manufactured by the Electro-Optics Division of the Bendix Co.). The operation of a Channeltron as a metastable detector has been described elsewhere[25] and will not be discussed here.

Metastable atoms and molecules produced in the interaction region were collimated by two 0.08-cm slits, located 7.5 and 12.3 cm away, before reaching the detector at a distance of 13.14 ± 0.24 cm. A pair of ceramic magnets placed behind the first slit provided a localized magnetic field of about 230 G. This field removed charged particles (protons from dissociative ionization and electrons from the electron gun) which could also be detected by the Channeltron. The magnetic field strength was well below the values (538 and 605 G) necessary to produce quenching of the $H(2S_{1/2})$ state owing to hyperfine level crossing between the $H(2S_{1/2})$ and $H(2P_{1/2})$[26,27] states. Calculations show that quenching effects caused by motional electric fields should not significantly affect the shape of the TOF distributions in this experiment.

Between the magnet pole faces were parallel plates (brass, 9-mm gap). By application of a strong electric field, the metastable hydrogen atoms could be completely quenched.

E. TOF Electronics

Figure 5 schematically illustrates how the TOF spectra were obtained. Initially, the electrons are pulsed on, enter the gas-filled interaction region, and produce metastable atoms. After a short delay (length of "on" pulse) a trigger pulse from the pulse generator starts a linear ramp voltage in the time-to-height converter (THC). A metastable atom, having travelled to the Channeltron via the slit system, produces a negative pulse in the Channeltron output. The pulse is amplified and shaped, and enters the THC stopping the ramp voltage. The THC output is a voltage pulse with peak height equal to the final ramp height. Thus, the output voltage of the THC is proportional to the time interval between the start and stop pulses which is in turn equal to (if we add the delay) the metastable atom's time of flight. This cycle was repeated at a frequency of about 5 kHz and the THC

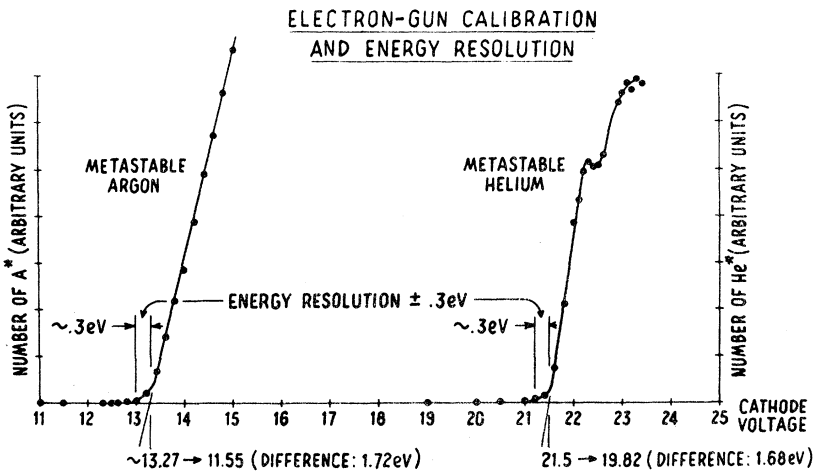

FIG. 4. Excitation functions for metastable helium and argon atoms. The width of the tail at threshold indicates the approximate half-width of electron energy spread. The voltage scale is calibrated by extrapolating the linear portion of the curves through the horizontal axis.

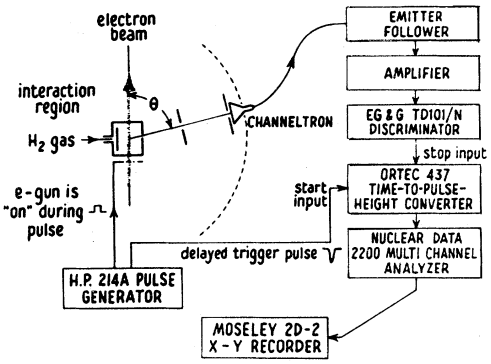

FIG. 5. Schematic of TOF electronics.

output was stored in a multichannel pulse-height analyzer. Afterward, a permanent graphic record was made by transferring the stored information to an X-Y recorder plot.

It should be noted that time intervals were measured up to the first detected H($2s$) atom and subsequent H($2s$) arrivals were ignored. The possible biasing of the TOF spectra in favor of the faster H($2s$) atoms was avoided, however, because of the low frequency of metastable atom arrivals (about one Channeltron pulse occurred for every ten pulses of the electron gun).

IV. EXPERIMENTAL RESULTS AND ANALYSES: MOMENTUM TRANSFER DURING COLLISION PROCESS

The angular distribution of H($2s$) atoms is governed not only by the processes discussed in Sec. II but also by the velocity distribution of the parent H_2 molecules and by the momentum transfer from the electron-molecule collision. In this experiment, an effort was made to assure that the ground-state molecules in the interaction region had an isotropic, Maxwellian distribution. Then, in order to understand the momentum-transfer effects, the angular distributions of metastable helium, neon, and molecular hydrogen were examined. No dissociation occurs for these metastable species and the angular distribution data will indicate how the isotropic ground-state distribution of the parent atom or molecule is modified by the collision process. These data are now examined.

A. Angular Distribution of Helium, Hydrogen (H_2), and Neon

The angular distributions for metastable helium ($2\,^3S_1$, $2\,^1S_0$), molecular hydrogen ($c\,^3\Pi_u$), and neon ($^3P_{2,0}$) are shown in Fig. 6. The electron energy was within 2 eV of the excitation threshold energy for each gas. The data were obtained by recording the TOF spectra for the various gases as a function of detector position. The TOF peak height was taken as a measure of metastable atom or molecule intensity (shifts in the peak position as a function of θ were small for $60° \leq \theta \leq 120°$). The data were also divided by source-chamber pressure (directly proportional to interaction region pressure) and electron-gun current to normalize for drifting of these parameters. The distributions were all normalized to unity at $\theta = 90°$.

To correct for changes in the interaction volume and losses due to collisional quenching and scattering as θ was varied, the data (except for neon for which n and σ were unknown) were multiplied by the factor $(\sin\theta)e^{n\sigma a\psi/\sin\theta}$. The determination of n, the density of ground-state gas in the interaction region, is described in the Appendix. The total cross section for removing a metastable atom from the beam is denoted by σ. The factor Ψ is also discussed in the Appendix.

The curves in Fig. 6 are calculated values of the metastable angular distribution for the various gases. The theoretical curves, developed by Pearl,[28] assume pure s-wave electron scattering during the collision process. This corresponds to isotropic scattering of the gas particles but with the inclusion of momentum-transfer effects from the electron. Further details of the calculation as well as the computer program for obtaining the curves as a function of atomic and molecular

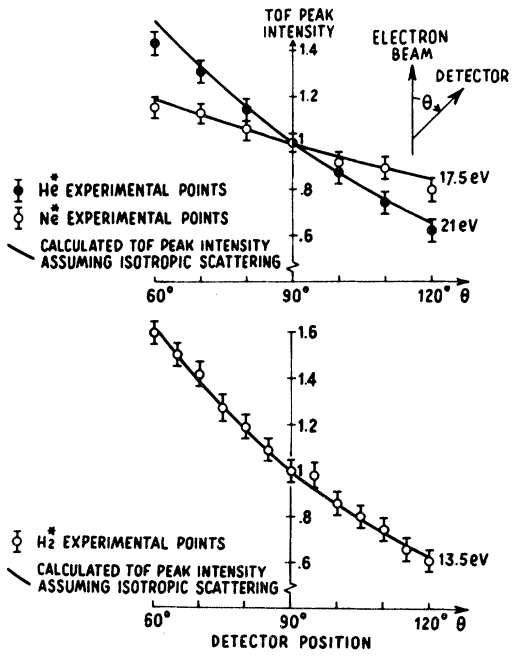

FIG. 6. Angular distributions of metastable helium, neon, and molecular hydrogen. The solid curves are calculated values of the angular distribution (Ref. 28) assuming pure s-wave scattering of the incident electron.

weight, gas temperature, excitation energy, and electron energy are given elsewhere.[29] The important result to note here is that what will be regarded as an "isotropic angular distribution" of *scattered* gas atoms or molecules is one that increases monotonically going from the backward to forward quadrants.

(*a*) *Helium*. The source density (n) and temperature (T) were near 4.4×10^{13} atoms/cm^3 and 140 °C, respectively. The source-chamber pressure (P_{sc}) was approximately 7×10^{-5} Torr while the detector-chamber pressure (P_d) was about 3.5×10^{-6} Torr. The cross section σ was taken[30] to be 1.65×10^{-14} cm^2. The factor $(\sin\theta)e^{n\sigma a\psi/\sin\theta}$ remains nearly constant for $60°\leq\theta\leq120°$. Comparing the helium data with the calculated angular distribution establishes that near threshold the helium metastable atoms are scattered isotropically.

(*b*) *Hydrogen* (H_2). The experimental conditions for the molecular hydrogen data were quite similar to those of helium. The values of n, T, P_{sc}, and P_d were 6.1×10^{13} molecules/cm^3, 105 °C, 8.6×10^{-5} Torr, and 4.3×10^{-6} Torr, respectively. No value for σ was found in the literature and it apparently remains to be measured. If the assumption is made that $(\sin\theta)e^{n\sigma a\psi/\sin\theta}$ is nearly constant (this is satisfied if $\sigma=1.60\times10^{-14}$ cm^2), the metastable H_2 angular distribution will be isotropic as can be seen by the excellent fit of the data in Fig. 6.

(*c*) *Neon*. Data were not taken to determine the value of n in the case of neon. The cross section σ is also unknown. The neon data of Fig. 6 was normalized to unity at $\theta=90°$ after having been divided by P_{sc} and electron-gun current. If one assumes that $(\sin\theta)e^{n\sigma a\psi/\sin\theta}$ is again approximately constant, the data indicate that neon is also scattered isotropically near its excitation threshold.

V. EXPERIMENTAL RESULTS AND ANALYSES: SLOW H(2*s*) ATOMS

With some understanding of the effects of momentum transfer during the collision process, we proceed now to an examination of data for the slow H(2*s*) atoms. The measurement and analyses of the angular distribution, threshold-energy, excitation-function, and energy distribution data of the slow H(2*s*) atoms will allow us to make assignments of several final excited states involved in the dissociative excitation process.

A. Threshold Energy and Excitation Function for Production of Slow H(2*s*) Atoms

The production of slow H(2*s*) atoms as a function of electron-gun voltage is shown in Fig. 7. In order to optimize the signal-to-noise ratio and eliminate the contribution from the metastable H_2 molecules [which overlaps with the low-energy tail of the H(2*s*) TOF spectrum], only H(2*s*) atoms which arrived at the detector between 10.8 and 22.5 μsec were observed. Thus, the slowest H(2*s*) atom fragment observed had a time of flight of 22.5 μsec or kinetic energy of ~0.16 eV. To eliminate background from the measured signal, the difference between Channeltron counts (integrated over several 10-sec intervals) with and without a 260-V/cm electric quench field was recorded; this is plotted on the vertical axes in Fig. 7. Each datum point was also divided by electron current and source-chamber pressure.

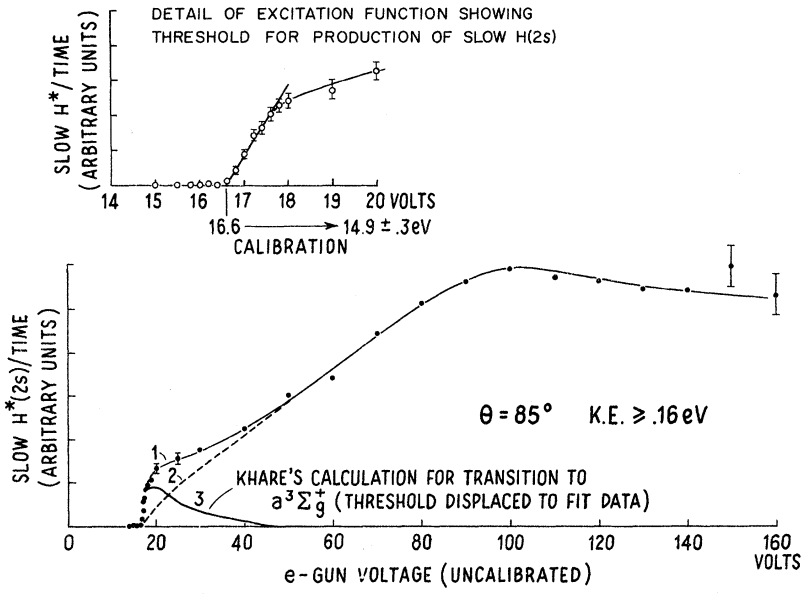

FIG. 7. Threshold energy for producing slow H(2*s*) atoms with 0.16 eV or more kinetic energy is 14.9±0.3 eV after calibration of the voltage scale. This places the asymptotic energy of the excited potential curves near 14.6 eV. The excitation function 1 can be decomposed into two curves representing cross sections for singlet-singlet transitions 2 and singlet-triplet transitions 3. The solid curve has been drawn to fit the data. The error bars indicate the statistical uncertainty ($\sqrt{N}$).

For the data shown in Fig. 7, the metastable atoms were observed at 85° with respect to the electron-beam direction. The threshold was observed to be independent of angle while the initial slope of the curve increased for smaller angles. This latter effect is kinematic in nature and is caused by the forward scattering of the parent molecule's center of mass after collision with the electron.

It can be seen from the threshold curve that H(2s) atoms with 0.16 eV or more kinetic energy are first produced at 14.9 ± 0.3 eV. Since momentum is conserved, each hydrogen atom of the molecule carries away an equal amount of kinetic energy and the total energy released is 0.32 eV or more. This places the asymptotic limit of the final-state potential energy curve(s) near 14.6 ± 0.3 eV which is the energy of two separated (noninteracting) H atoms in the H(1s) and H(2s or 2p) states.[31]

The experimental excitation function for producing slow H(2s) atoms is shown at the bottom of Fig. 7 (curve 1). It can be decomposed into a sum of two excitation functions, one representing a transition with a rapid rise and fall in cross section (curve 3) and the other with a more gradual increase (curve 2). The rapid rise and fall of curve 3 is characteristic of a singlet-triplet transition and Khare's[32] calculated cross section for excitation to the $a^3\Sigma_g^+$ state has been sketched in to represent this kind of transition.[33] When Khare's theoretical curve is subtracted from the experimental curve, the more slowly changing excitation function, curve 2, is obtained. The slow rise and fall of curve 2 characterizes a singlet-singlet transition and resembles the singlet-singlet cross sections calculated by Khare.[34] Therefore, it would appear that when the slow H(2s) atoms are produced, transitions to a triplet state(s) dominates initially while at higher electron energies, transitions occur primarily to a singlet state(s).

B. Energy Distribution of Slow H(2s) Atoms

It was noted earlier that there is some disagreement in the literature regarding the energy distribution of the slow H(2s) atoms. Leventhal *et al.*[1] observed that the relative number of very-low-kinetic-energy H(2s) atoms was less than that predicted by the theoretical calculations of Harriman.[6] This was considered as possible evidence for energy barriers in the final-state potential curves.

More recently, Clampitt and Newton,[2] using an arrangement where an H_2 beam was crossed with the electron beam, also examined the TOF spectrum of the slow H(2s) atoms. Their results, when transformed to energy coordinates, were essentially in agreement with the Harriman prediction. Clampitt and Newton speculated that a possible cause for the difference in experimental results might be in the method of detection. Leventhal *et al.* observed the H(2s) atoms by quenching them with a dc electric field and counting the Lyman-α photons, while Clampitt and Newton detected the H(2s) atoms through an Auger process on an electron-multiplier cathode.

During the present study, the TOF distribution of H(2s) atoms was measured directly with a Channeltron electron multiplier and transformed to an energy distribution.[35] A typical experimental energy distribution is shown in Fig. 8(a). The spectrum was obtained with 80-eV electrons (production of metastable H_2 is negligible at this electron energy) with $\theta = 80°$. The uncertainty in the kinetic energy is due to a 0.5-μsec electron pulse width and to an uncertainty in the length of the flight path. The vertical error bars, shown at representative points, are statistical in nature. The relatively large vertical error bars shown at low kinetic energies results from the properties of the transformation.[35] Thermal motion of the parent molecules contributes to the width of the measured energy distribution. The energy distribution is in approximate agreement with the re-

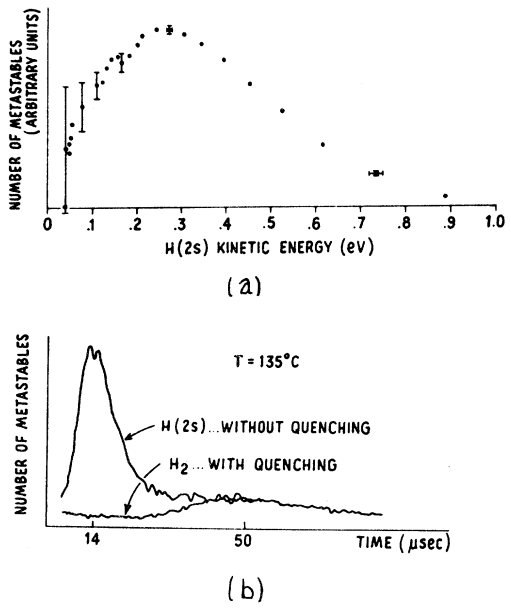

FIG. 8. (a) Energy distribution of slow H(2s) atoms obtained with 80-eV electrons ($\theta = 80°$) shows a low-energy cutoff as observed by Leventhal *et al.* (b) A comparison of TOF spectra obtained with 38-eV electrons ($\theta = 90°$) with and without an electric quench field shows a presence of metastable H_2 molecules; when the molecular contribution is subtracted from the unquenched TOF spectrum, a low-energy cutoff of H(2s) atoms is again observed.

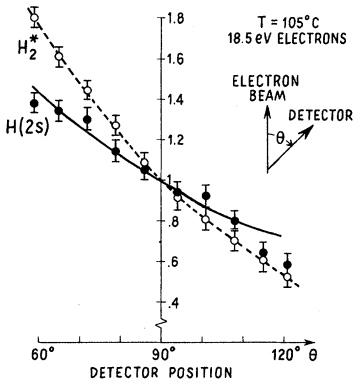

FIG. 9. Angular distribution of metastable H_2 and ~0.4-eV H(2s) atoms. The angular distribution of the atoms is approximately isotropic; the departure from a constant intensity for different values of θ is due to momentum transfer during the collision process. The solid curve is a calculated distribution and is discussed in Ref. 45.

sults of Leventhal *et al.*[1] (i.e., there is a low-energy cutoff) with a slight shift to the lower end of the energy scale in the present case.

The possible loss of low-energy H(2s) atoms because of preferred collisional quenching was examined by varying the source pressure from about 1.5×10^{-4} to 3×10^{-3} Torr. The shape of the TOF spectra remained unchanged.

Time-of-flight spectra were also obtained with 38-eV electrons in order to make a comparison with the results of Clampitt and Newton. Figure 8(b) shows tracings of TOF spectra with and without the electric quench field at $\theta = 90°$. The trace with no electric quenching field exhibits a peak near 14 μsec owing to the slow H(2s) atoms. When the quench field is turned on, a trace of just the metastable H_2 molecules is observed with a peak near 50 μsec. In contrast to the results of Clampitt and Newton, these results show that the cross section for producing metastable H_2 is not negligible for 38-eV electrons. When the contribution of the molecules is subtracted from the "tail" of the slow H(2s) distribution, the deficiency of low-energy H(2s) atoms is evident. Thus the earlier results of Leventhal *et al.* were again observed.

C. Angular Distribution of Slow H(2s) Atoms

Figure 9 shows the angular distribution for the slow H(2s) atoms with kinetic energies of about 0.4 eV. The angular distribution of the metastable H_2 molecule (thermal energies) is also shown for comparison. Both curves are obtained with 18.5-eV electrons, which is near the threshold energy for producing the slow H(2s) atoms (Sec. V A). The respective TOF peak heights were again taken as a measure of intensity. The data were multiplied by $(\sin\theta)e^{n\sigma a\psi/\sin\theta}$ and divided by the electron-gun current and source-chamber pressure. The value of σ for H(2s) atoms with kinetic energy near 0.4 eV was taken[36] as 2×10^{-14} cm^2.

The laboratory angular distribution of slow H(2s) atoms can be interpreted as being approximately isotropic because of its resemblance to the data in Fig. 6. The fragment distribution would be constant (horizontal line) if momentum-transfer effects were negligible. With inclusion of momentum-transfer effects, one might intuitively expect a lifting of the center-of-mass distribution in the forward quadrant and lowering in the backward quadrant. While this conclusion is correct, one must use caution in applying this argument since its validity can be shown to depend on the range of fragment velocities that are accepted in the measurement.[22]

D. Processes and States Leading to Slow H(2s) Atoms

The interpretation of the excitation function and angular distribution to identify the final states is now discussed. One must consider both dissociation (a relatively fast process that leads to an angular distribution of fragments indicative of the molecule's orientation at the time of electron impact) and predissociation (a process that may take a time that is appreciable when compared to the rotation time of the molecule). Both processes appear to contribute to the data found in this experiment.

1. Dissociation

Of the many states in H_2 that can be excited by electrons of 15–20 eV, only the $E\,^1\Sigma_g^+$, $a\,^3\Sigma_g^+$, $B'\,^1\Sigma_u^+$, and $e\,^3\Sigma_u$ states lead directly to H(1s) +H(2s) in the separated atoms limit.[31] Since Dunn's rules[11] indicate that only $\Sigma_g^+ \rightarrow \Sigma_g^+$ transitions can occur for both parallel and perpendicular orientations, and since both orientations are required to produce an isotropic distribution of atoms (assuming for the moment that no predissociation occurs), it was at first[37] thought that the $E\,^1\Sigma_g^+$ and $a\,^3\Sigma_g^+$ states were involved in the production of the slow H(2s) atoms. However, the repulsive portion of the potential curves of the E and a states are located in the fringe of the Franck-Condon region (Fig. 10), so we conclude these states are not prime sources of the slow H(2s) atoms.

It can be seen that the repulsive portions of the B' and e potential curves do occupy a fairly central portion in the Franck-Condon region. But Dunn's rules suggest that transitions to these Σ_u^+ states are possible near threshold only for parallel orientations of the molecular axis; thus the dissociation via B' and e states would yield a $\cos^2\theta$ distribution of fragments with a minimum at 90°. Dissociation may occur with significant probability,

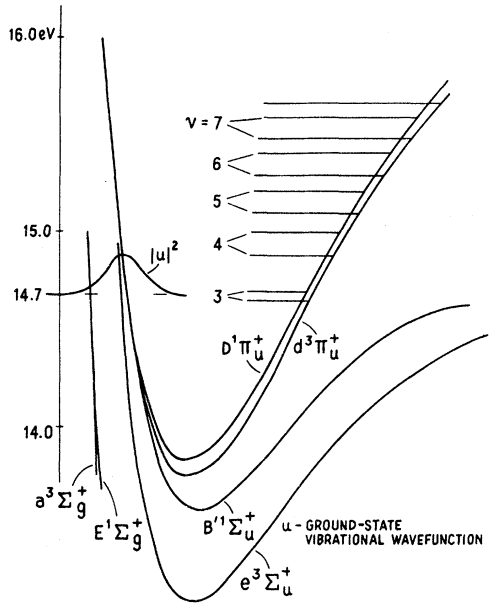

FIG. 10. Some energy levels of H_2 near 15 eV after Sharp (Ref. 31). The $a\,^3\Sigma_g^+$ and $E\,^1\Sigma_g^+$ states are located in the fringe of the Franck-Condon region making large contributions of H(2s) atoms from these states unlikely. The D, d, B', and e states are more favorably located and are expected to play a predominant role in the production of slow H(2s) atoms. The ground-state vibrational wave function u is taken from Ref. 6.

but it appears that dissociation by itself cannot explain the observed isotropic distribution of slow H(2s) atoms.

2. *Predissociation*

On the basis of small Franck-Condon overlap integrals, it appears that the $E\,^1\Sigma_g^+$ and $a\,^3\Sigma_g^+$ states do not participate to any extent in the predissociation process. Thus the predissociating states must mix with the $B'\,^1\Sigma_u^+$ or the $e\,^3\Sigma_u^+$ states as the molecule goes to the H(1s)+H(2s) separated-atoms limit. Of the states that can be excited with electrons of less than 20 eV, only a few meet the criteria for making a mixing transition to the B' or e states. Since $g \nleftrightarrow u$ in a mixing transition, the predissociating state must be ungerade; since $\Delta\Lambda = 0, \pm 1$, the predissociating state must be Σ or Π. Also, singlet-triplet transitions are not allowed in mixing of the sort being considered here.

The most important states in the production of slow H(2s) atoms by predissociation are $D\,^1\Pi_u^+$ and $d\,^3\Pi_u^+$. The D and B' states are known[3,38,39] to be mixed by strong rotational perturbations, and the mixing of the d and e states has also been demonstrated.[40] We note that these pairs of states (D and B', d and e) have merging potential curves, go to the same united atom limit of He $^{1,3}P(1s3p)$, and satisfy the selection rules for mixing transitions.

Some contribution to the slow H(2s) atoms probably comes from the vibrationally excited levels of the $B''\,^1\Sigma_u^+$ state. Comes and Wenning[41] have shown that $B''(v=1)$ mixes with the B' level above the dissociative limit; the relative line intensities in their data suggest that $B''(v=1)$ is less important than $D(v=3)$ in predissociation. It is likely that the $v>1$ levels of the B'' state also predissociate, but spectroscopic evidence for this is difficult to obtain because of the near coincidence of these levels with the $v>3$ levels of the $D\,^1\Pi_u$ state.[42] The triplet state that corresponds to the singlet B'' is $f\,^3\Sigma_u^+$; it may predissociate but we are unaware of any direct evidence for this.

Still smaller contributions to the slow H(2s) atoms might arise from the $D'\,^1\Pi_u$ state that is believed to mix weakly with the repulsive portion of the B' state near the dissociative limit.[38]

Finally there are a number of states excited by electron bombardment that probably do *not* predissociate into H(1s)+H(2s). Since the potentials of of the h, H, g, G, and 0 Σ_g^+ states do not merge with either the B' or the e potentials, their Franck-Condon factors seem unfavorable, and their predissociation would require a violation of the $g \nleftrightarrow u$ selection rule. The potential of the $B\,^1\Sigma_u^+$ state does not merge with that of the B' state; in fact the $B\,^1\Sigma_u^+$ state is known[43] to mix strongly with the $C\,^1\Pi_u$ state and this mixture will not lead to H(2s) atoms. The behavior of the $b\,^3\Sigma_u^+$ and $c\,^3\Pi_u$ states is expected[44] to resemble that of B and C.

E. Summary: Production of Slow H(2s) Atoms

Near threshold, the important processes in the production of slow metastable H atoms are dissociation via a parallel transition to the $e\,^3\Sigma_u^+$ state, along with predissociation via a perpendicular transition to the $d\,^3\Pi_u$ state that subsequently mixes with the e state.

Above threshold, the important processes are dissociation via a parallel transition to the $B'\,^1\Sigma_u^+$ state, and predissocation via a perpendicular transition to the $D\,^1\Pi_u$ state that subsequently mixes with the B' state. [Some predissociation also occurs via a parallel transition to the $B''\,^1\Sigma_u^+$ ($v>0$) states.]

Dissociation at and near threshold occurs primarily through parallel transitions and therefore yields fragments with approximately a $\cos^2\theta$ dependence. Predissociation at and near threshold occurs mainly through perpendicular transitions; the process is relatively slow and it leads to dissociation fragments with an angular distribution proportional to $3 - \cos^2\theta$. The observed isotropy of the fragments then suggests that predissociation is the dominant[45] but not exclusive process in the production of slow H(2s) atoms.

F. Discussion

Because of the discreteness of the $D\,^1\Pi_u^+$ vibrational levels and the large contributions from predissociation near these points,[39] one would expect to see structure in the energy distribution of H(2s) atoms (a similar contribution would be expected from $d\,^3\Pi_u^+$ vibrational levels). The number of "wiggles" in the energy distribution would decrease at higher electron energies as the cross section for excitation to the vibrational levels of the triplet Π_u state became smaller. The spectroscopic data of Mentall and Gentieu[39] imply that structure from the predissociation of the $D\,^1\Pi_u^+(v=3, 4, 5, 6, 7)$ levels occurs in the H(2s) energy distribution near 0.05, 0.15, 0.26, 0.36, 0.45 eV and possibly higher. The energy spectrum of Fig. 8(a), obtained with 80-eV electrons, shows no structure, but this is because of the spreading of translational kinetic energy because of the thermal motion of the parent molecules.[46]

Structure in the H(2s)-atom TOF distribution was observed by Czarnik and Fairchild[3] who obtained TOF spectra with their H_2-gas target cooled to an estimated 50 °K; they used 32-eV electrons to excite the molecules. We agree with their statement that predissociation of the $D\,^1\Pi_u$ state is an important process in the production of slow H(2s) atoms. We disagree with their conclusions that predissociation of Rydberg states [e.g., $8p\sigma\,^1\Sigma_u^+(v=5)$] through doubly excited states [e.g., $(2s\sigma)(2p\sigma)\,^1\Sigma_u^+$] contributes to the production of slow H(2s) atoms; in fact it appears that these doubly excited states are responsible for the production of fast hydrogen atoms (cf. Sec. VI B). Moreover, it seems likely that predissociation from vibrational levels of the $d\,^3\Pi_u$ state would contribute to their experiment; from our data we estimate (see Fig. 7) that about one-third of the dissociative excitations leading to slow H(2s) atoms that are produced by 30-eV electrons do so by exciting the $d\,^3\Pi_u^+$ state. It is noted that Czarnik and Fairchild have assigned an apparent peak in the TOF distribution at 0.13 eV to predissociation of the $D\,^1\Pi_u^+(v=3)$ level. This is about twice the expected energy value of 0.05 eV. A possible alternate assignment for this structure would be the predissociation of the $d\,^3\Pi_u(v=4)$ level expected to produce H(2s) atoms with 0.1-eV kinetic energy.[31]

What remains unexplained is the deficiency of low-kinetic-energy H(2s) atoms in the energy distribution. The data of Mentall and Gentieu (their Fig. 4 and private communication) indicates that H(2s) atoms with nearly zero kinetic energy are produced by predissociation of the $D\,^1\Pi_u^+(v=3)$ level after the D state is optically excited (see Fig. 10). Their data also show that collisional quenching of H(2s) atoms changes sharply in the pressure range (0.5×10^{-3})–(4×10^{-3}) Torr. This contrasts with results in Fig. 8(a) [no H(2s) atoms with ~ zero kinetic energy] and the observation that the TOF spectra showed no measurable change in the number of low-energy H(2s) atoms when recorded at 0.15×10^{-3} and 3×10^{-3} Torr. Slow H(2s) atoms are particularly susceptible to quenching by stray electric fields, and the possibility that slow atoms were quenched cannot be ruled out completely. However, there appears to be no ready explanation for the lower abundance of slow H(2s) atoms as measured in the present experiment and in the experiment by Leventhal, Robiscoe, and Lea[1] as compared to the results obtained in the experiments of Clampitt and Newton[2] and of Mentall and Gentieu.[39]

VI. EXPERIMENTAL RESULTS AND ANALYSES: FAST H(2s) ATOMS

A. Angular Distribution of Fast H(2s) Atoms

Figure 11 shows the angular distribution of fast H(2s) atoms with kinetic energies near 3.7 eV. The electron energy was about 41.5 eV and the TOF peak height was again used as a measure of intensity. The data were normalized as before with the value[47] of σ being taken as 2×10^{-14} cm^2. The points in Fig. 11 represent data from two different experimental runs. While the electron energy of 41.5 eV is somewhat above the threshold energy of 32 eV (see Sec. VI B), the change in the angular distribution was observed to be gradual as the electron energy was increased (see Fig. 12). Thus Fig. 11 gives a fair approximation of how the angular distribution appears at threshold. The distribution can be interpreted as one that would be symmetrically peaked at $\theta=90°$ if the ef-

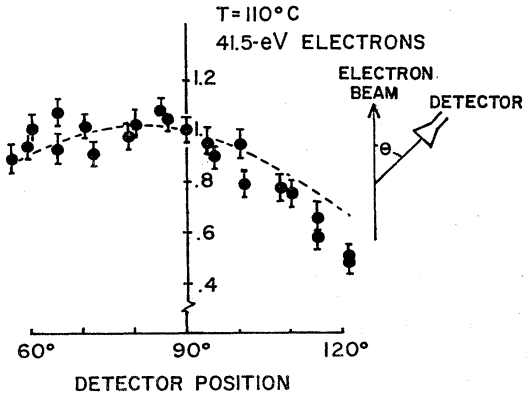

FIG. 11. Angular distribution of fast H(2s) atoms with ~3.7-eV kinetic energy. The angular distribution can be interpreted as representing a $\Delta\Lambda\neq0$ transition; a calculated distribution is shown as a dashed curve (see text).

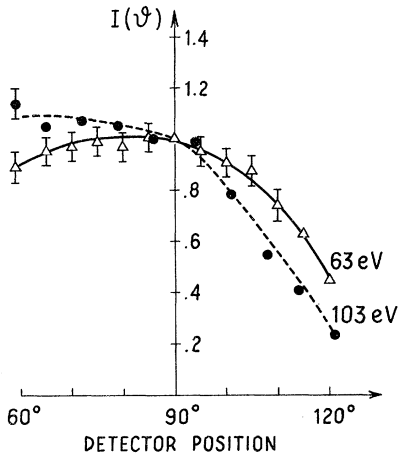

FIG. 12. Behavior of fast-H(2s) atom (~3.7-eV kinetic energy) angular distributions produced with electrons having 63- (Δ) and 103-eV (○) energy. The value of β (cf. Sec. II A 2) is expected to increase with electron energy making the center-of-mass angular distribution more isotropic. These data suggest that the component of momentum transfer along the electron beam has increased. For the fragment velocity observed, this leads to greater lifting of the center-of-mass angular distribution in the forward quadrant and lowering in the backward quadrant. The curves are drawn to fit the data.

fects of momentum transfer had been negligible (cf. Sec. V C). The dashed curve in Fig. 11 is a calculated[22] laboratory angular distribution using Eq. (6) ($\Delta\Lambda = 1$) with $\beta = 25°$ as the center-of-mass angular distribution; the fragment energy was taken to be 4 eV. A rough estimation of the Franck-Condon factors was made from a fast-H(2s)-atom energy distribution observed at 41.5-eV electron energy. The calculated curve is seen to be in qualitative agreement with the data. According to Dunn's table (Fig. 2), such "perpendicular" transitions can occur to Π_u- and Δ_g-type electronic states. Thus, the final parent molecular state(s) which yields the fast H(2S) atoms can be narrowed down to these two possibilities.

B. Threshold Energy and Excitation Function for Producing Fast H(2s) Atoms

The production of fast H(2s) atoms as a function of electron gun voltage is shown in Fig. 13. The data were obtained by recording TOF spectra for increasing electron energies. The height of each TOF spectrum at one point in time, corresponding to an approximate[48] kinetic energy of 3.8 eV, was measured and plotted after dividing by electron current and source-chamber pressure. The TOF spectra were taken at $\theta = 80°$. The threshold energy appeared to be independent of angle while the initial slope of the excitation function increased as θ was decreased.

It can be seen from the threshold curve that H(2s) atoms with ~3.8-eV kinetic energy are first produced at 32 eV. The asymptotic limit for the potential energy curve can be determined by subtracting 2×3.8 eV, the total kinetic energy released, from the threshold energy of 32 eV. This places the asymptotic limit at around 24.4 eV which is close to the 24.9-eV energy for the doubly excited separated-atom configurations of H(2s) +H(2s) and H(2s)+H(2p). This interpretation is further supported by the observation that the least

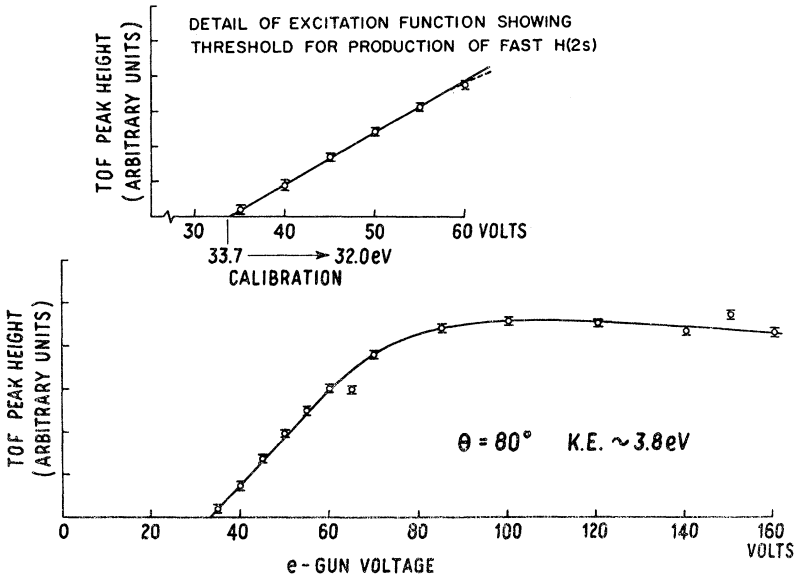

FIG. 13. Peak of the TOF spectrum for fast H(2s) atoms plotted as a function of electron energy. The threshold energy for producing fast H(2s) atoms with ~3.8-eV kinetic energy is 32 eV after calibration of the energy scale. This places the asymptotic energy of the excited potential curve near 24.9 eV. The excitation function appears to represent a singlet-singlet transition. The solid curve has been drawn to fit the data. Departures from the curve near 60 and 150 eV are not reproducible.

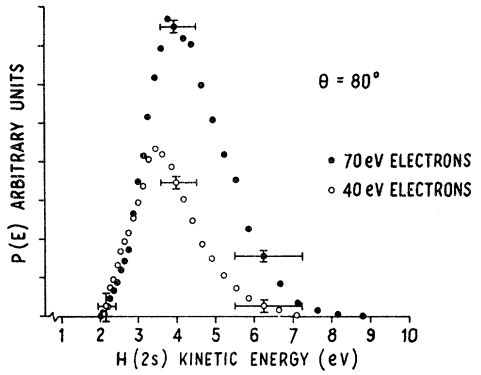

FIG. 14. Energy distribution of fast H(2s) atoms for 40- and 70-eV electrons.

energetic of the fast H(2s) atoms have a kinetic energy of slightly in excess of 2 eV (see Sec. VIC) and are first observed near 29 eV.

It had previously been speculated[1] that $(2s\sigma)\times(2p\sigma)^{1,3}\Sigma_u^+$ states with potential curves asymptotically approaching 14.7 eV were responsible for producing the fast H(2s) atoms. Czarnik and Fairchild[3] suggested that these were the perturbing states through which the $9p\sigma\,^1\Sigma_u^+(v=5$ at 16.46 eV), $8p\sigma\,^1\Sigma_u^+(v=5$ at 16.41 eV), and $8p\sigma\,^3\Sigma_u^+(v=4$ at 16.20 eV) levels predissociated and led to slow H(2s) atoms. We note that the potential energy curve leading to the fast H(2s) atoms will likely remain well above 16.5 eV (Sec. VID and Fig. 15) and will not be able to play a role in the production of the slow H(2s) atoms.

The shape of the excitation function shows no apparent superposition of transitions between states of different multiplicities but rather has a gradual rise and fall characteristic of a singlet-singlet transition.

C. Energy Distribution of Fast H(2s) Atoms

Time-of-flight spectra of the fast H(2s) atoms, taken as a function of electron energy, were converted to energy distributions. Two energy distributions obtained with 40- and 70-eV electrons at $\theta=80°$ and $T=120\,°C$ are shown in Fig. 14. As the electron energy is increased, the peak position is shifted to higher energy values and H(2s) atoms with larger kinetic energy are produced. At 70 eV the most probable energy is near 4.0 ± 0.6 eV, which is close to the value observed by Leventhal *et al.*[1] (4.7 ± 0.7 eV). The uncertainty in the energy scale in Fig. 14 is due to the electron pulse width (0.4 μsec) and uncertainty in the path length (±0.24 cm). Effects of thermal broadening are included which means that the slowest H(2s) atoms from the dissociation process are likely to have energies near 2.3 eV instead of 2 eV.[48]

The structure that Leventhal *et al.* observed in the fast H(2s) TOF spectra at $\theta=77°$ could not be seen in the present work. An explanation for the difference in results is not apparent.

D. Final States in Production of Fast H(2s) Atoms

The analysis of the fast H(2s) data does not appear to be as involved as the slow-H(2s)-atom case, The behavior of the H(2s)-atom energy distribution as a function of electron energy (Fig. 14) would be expected for a transition to the repulsive portion of an excited potential.

The angular distribution data near threshold suggests that the final states can be of the Π_u and Δ_g types and the shape of the excitation function indicates a multiplicity of one. The asymptotic limit of the potential curves is most likely 24.9 eV which is the separated-atom energy for the H(2s) +H(2s) and H(2s)+H(2p) configurations.

The Δ_g choice must be rejected because of two arguments: (a) The lowest asymptotic energy for a doubly excited adiabatic Δ_g state is 26.8 eV formed from H(2s)+H(3d) atoms. This energy is too large when compared with the experimental value. (b) The cross section for producing fast H(2s) atoms remains relatively large at higher electron energies where the transition probability is a function of $\langle\vec{M}\rangle$, the dipole matrix element (Sec. II). A $X\,^1\Sigma_g^+\rightarrow\Delta_g$ transition would not be allowed because of the dipole selection rules $g\not\rightarrow g$ and $\Delta\Lambda=0,\pm1$.

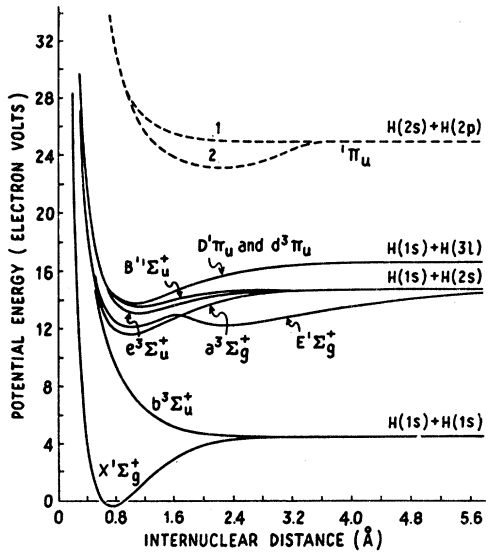

FIG. 15. Potential energy diagram of H_2 after Ref. 31 showing several excited states. The approximate location of the $^1\Pi_u$ states discussed in the text has been added near the top of the figure. Whether this state is purely repulsive (curve 1) or bound (curve 2) cannot be determined from the data.

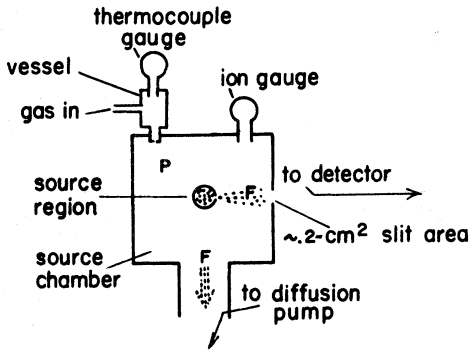

FIG. 16. Schematic view of source chamber and source (interaction) region.

This means that the final state leading to the fast H(2s) atoms is a $^1\Pi_u$ state. This state is formed from H(2s)+H(2p) atoms since a Π state cannot be formed from two H(2s) atoms. The approximate location of the potential curve is indicated near the top of Fig. 15. It is noteworthy that this state has not been previously reported in the literature. The detailed behavior of the potential curve awaits further experimental study as well as a theoretical calculation.

ACKNOWLEDGMENTS

We are grateful to Professor R. T. Robiscoe for initiating the research and for his many contributions to the early stages of the experiment. We are indebted to B. Babcock for help in the design and construction of the apparatus. We thank J. Pearl, T. E. Sharp, and R. Freund for many helpful discussions. A portion of the analyses was performed by MM during tenure as a NRC Postdoctoral Resident Research Associate at Goddard Space Flight Center, Greenbelt, Md.

APPENDIX: SOURCE DENSITY AND BEAM ATTENUATION

Source Density

Because of the inaccessibility of the source region (interaction region of electron gun), an indirect method was devised to measure the source density. The method makes use of the well-known definition of pumping speed

$$S = F/P \,, \tag{A1}$$

where P is the pressure in the source chamber and F is the number of gas particles being pumped out of the source chamber per second. When the system is in equilibrium, F can also be thought of as the input of molecules into the source chamber from the source region (see Fig. 16). The approximation is made that effusion from the source region is roughly that from an orifice. The input from the source region is then given by[49]

$$F = \tfrac{1}{4} nvA \,, \tag{A2}$$

where n is the density of gas in the source region, v is the average molecular speed in the source [given by $v = (2.55kT/m)^{1/2}$], and A is the area of the opening. Equation (A1) can then be written

$$S = F/P = nvA/4P \,, \tag{A3a}$$

or solving for n,

$$n = 4SP/vA \,. \tag{A3b}$$

Therefore, if one knows the pumping speed and and pressure P for the source chamber as well as A and v, the value of the source density n can be calculated. The values of A, P, and T are readily measured. The pumping speed of the source chamber for a particular gas was determined by injecting a known flux[50] of the gas into the source chamber, measuring P with an ionization gauge, and then calculating S using Eq. (A3a). The value of S was found to be about 178 liters/sec for hydrogen and 130 liters/sec for helium.

TABLE I. Values of Ψ.

v/α	$\Psi(v/\alpha)$
0.05	22.586
0.1	11.321
0.2	5.717
0.4	2.969
0.6	2.099
0.8	1.694
1.0	1.472
2.0	1.125
3.0	1.056

Beam Attenuation

As the detector position was changed from $\theta = 90°$, the path length l of the metastable atoms in the source region increased as $l = a/\sin\theta$, where a

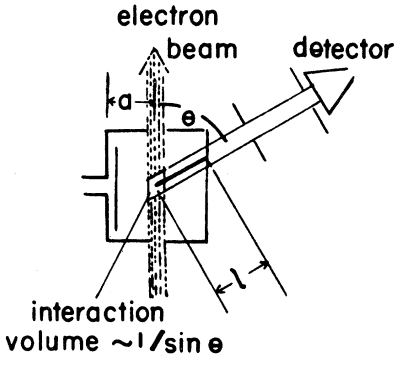

FIG. 17. Interaction region of electron gun.

is the radius of the source region (see Fig. 17). Because of the high density of gas in the source region, this led to greater beam attenuation from collisions.

The loss from collisions is also a function of velocity and the fraction of metastable atoms having speed v which remain in the beam after traveling a distance l through a Maxwellian gas is[51,52]

$$e^{-n\sigma l\Psi(v/\alpha)},$$

where σ is the total cross section for removing a metastable atom from the beam (assumed velocity independent), α is the most probable speed of the gas in the source region, and Ψ is a function of v/α. The value of the Ψ factor increases for smaller v and reflects the greater likelihood of collision for slower metastable atoms passing through a Maxwellian gas. Some values of $\Psi(v/\alpha)$ are given in Table I; it can be seen that Ψ varies markedly for thermal-beam velocities.

An effect which competes with beam attenuation is the angular dependence of the actual interaction volume. Assuming a parallel beam of electrons, it can be seen from Fig. 17 that the interaction volume has a $1/\sin\theta$ dependence. To correct for this effect as well as collision attenuation, each data point was multiplied by $(\sin\theta)e^{n\sigma a\Psi/\sin\theta}$.

---

*Work supported in part by the U. S. AEC under Grant No. AT-11-1-1112 and by NASA under Grants No. NAS-8-21267 and NAS-8-21450.

†Present address: Goddard Space Flight Center, Code 691, Greenbelt, Md. 20771.

[1]M. Leventhal, R. T. Robiscoe, and K. R. Lea, Phys. Rev. 158, 49 (1967).

[2]R. Clampitt and A. Newton, J. Chem. Phys. 50, 1997 (1969); R. Clampitt, Phys. Letters 28A, 581 (1969).

[3]J. W. Czarnik and C. E. Fairchild, Phys. Rev. Letters 26, 807 (1971).

[4]M. Misakian and J. C. Zorn, Phys. Rev. Letters 27, 174 (1971).

[5]E. U. Condon, Phys. Rev. 32, 858 (1928).

[6]J. M. Harriman, Ph. D. thesis (Stanford University, 1956) (unpublished), available from Xerox-University Microfilms, Inc. Ann Arbor, Mich., Publication No. 20450.

[7]J. G. Winans and E. C. G. Stueckelberg, Proc. Natl. Acad. Sci. (U.S.) 14, 867 (1928).

[8]A. S. Coolidge, H. M. James, and R. D. Present, J. Chem. Phys. 4, 193 (1936).

[9]L. J. Kieffer and Gordon H. Dunn, Phys. Rev. 158, 61 (1967).

[10]P. J. Chantry and G. J. Schulz, Phys. Rev. 156, 134 (1967).

[11]G. H. Dunn, Phys. Rev. Letters 8, 62 (1962).

[12]R. N. Zare and D. R. Herschbach, Proc. IEEE 51, 173 (1963); R. N. Zare and D. R. Herschbach, UCRL Report No. 10438, 1962 (unpublished).

[13]H. S. W. Massey, *Encyclopedia of Physics*, edited by S. Flügge (Springer, Berlin, 1956), Vol. 36, p. 355.

[14]V. N. Sasaki and T. Nakao, Proc. Imp. Acad. Japan 11, 138 (1935); 17, 75 (1941).

[15]G. H. Dunn and L. J. Kieffer, Phys. Rev. 132, 2109 (1963).

[16]R. J. Van Brunt and L. J. Kieffer, Phys. Rev. A 2, 1293 (1970).

[17]R. N. Zare, J. Chem. Phys. 47, 204 (1967).

[18]The electronic eigenfunctions given by Π_g, Σ_u, etc., are solutions of the H_2 Hamiltonian describing the molecule with both nuclei fixed in space. When the interaction of the electronic and nuclear motions are considered, it is found that the rotational and vibrational motions of the nuclei act as perturbations which can mix electronic states of the same total angular momentum J, parity (+ or −), symmetry ($g \nleftrightarrow g$, $u \nleftrightarrow u$, $g \leftrightarrow u$), and spin S. Electronic states which interact because of vibrational motion (homogeneous perturbation) are characterized by $\Delta\Lambda = 0$ and for the case of rotational motion (heterogeneous perturbation), $\Delta\Lambda = \pm 1$; see, for instance, G. W. King, *Spectroscopy and Molecular Structure* (Holt, New York, 1964), pp. 242 ff.

[19]R. S. Berry and S. E. Nielson, Phys. Rev. A 1, 395 (1970).

[20]Paul S. Julienne, Chem. Phys. Letters 8, 27 (1971).

[21]C. Jonah, J. Chem. Phys. 55, 1915 (1971). An earlier quantum-mechanical treatment of the problem has been made by R. N. Zare, Ph. D. thesis (Harvard University, 1964) (unpublished). See also G. E. Busch and K. R. Wilson, J. Chem. Phys. 56, 3638 (1972).

[22]A detailed treatment of linear-momentum-transfer effects in molecular dissociation by electron impact has been made recently by M. Misakian, J. C. Pearl, and M. J. Mumma [J. Chem. Phys. 57, 1891 (1972)].

[23]R. H. McFarland, Phys. Rev. 133, A986 (1964).

[24]R. E. Fox, W. M. Hickman, D. J. Grove, and T. Kjeldass, Jr., Rev. Sci. Instr. 26, 1101 (1955).

[25]D. P. Donnelly, J. C. Pearl, R. A. Heppner, and J. C. Zorn, Rev. Sci. Instr. 40, 1242 (1969).

[26]W. E. Lamb, Jr. and R. C. Retherford, Phys. Rev. 79, 549 (1950); 81, 222 (1951).

[27]R. T. Robiscoe, Phys. Rev. 138, A22 (1965).

[28]J. C. Pearl, Ph. D. dissertation (University of Michigan, 1970) (unpublished), available from Xerox-University Microfilms, Inc., Ann Arbor, Mich.

[29]Martin Misakian, Ph. D. dissertation, (University of Michigan, 1971) (unpublished), available from Xerox-University Microfilms, Inc., Ann Arbor, Mich.

[30]R. G. Stebbings, Proc. Roy. Soc. (London) A241, 270 (1957).

[31]T. E. Sharp, At. Data 2, 119 (1971).

[32]S. P. Khare, Phys. Rev. 157, 107 (1967).

[33]The peak height of Khare's curve has been arbitrarily normalized to produce a smooth decomposition of the experimental data and the threshold has been displaced from 11.7 (production of photons) to 14.6 eV (production of atom fragments).

[34]S. P. Khare, Phys. Rev. 149, 33 (1966).

[35]The transformation from a time-of-flight to an energy distribution is made using the relations $P(E)\,dE = P(t)\,dt$ and $E = mL^2/2t^2$, where L is the path length, m is the atomic mass, and t is the time of flight. The energy distribution is just $P(E) = P(t)\,dt/dE = P(t)t^3/mL^2$.

[36]F. J. Comes and U. Wenning, Z. Naturforsch. 24a, 587 (1969).

[37]Martin Misakian, in Proceedings of the Twenty-Fifth Symposium on Molecular Structure and Spectroscopy, Columbus, Ohio, 1970 (unpublished).

[38]T. Namioka, J. Chem. Phys. 41, 2142 (1964).

[39]J. E. Mentall and E. P. Gentieu, J. Chem. Phys. 52, 5641 (1970).

[40]G. H. Dieke, Phys. Rev. 48, 610 (1935).

[41]F. J. Comes and U. Wenning, Z. Naturforsch. 25a, 237 (1970).

[42]A. Monfils, J. Mol. Spectry. 15, 265 (1965).

[43]T. Namioka, J. Chem. Phys. 40, 3154 (1964).

[44]The C, c, B, and b states all go to the same energy level (He $^{1,3}P1s2p$) in the united-atom approximation (see Ref. 31) and consequently the respective potential curves will merge as the internuclear distance decreases. The crossing of the levels permits the mixing.

[45]Using the methods outlined in Ref. 22, laboratory angular distributions for the present experiment were calculated (a) for direct dissociation of the $e\,^3\Sigma_u^+$ state using Eq. (5) with $\beta = 20°$ to describe the center-of-mass angular distribution, and (b) for predissociation of the $v = 4$, 5, 6, and 7 levels of the $d\,^3\Pi_u$ state assuming the angular distribution to be proportional to $3 - \cos^2\theta$. In both cases the dissociation fragments were assumed to have a laboratory kinetic energy of 0.5 eV. The Franck-Condon factors and relative contributions from the $v = 4$, 5, 6, and 7 levels were estimated crudely from an energy distribution of slow H(2s) atoms measured at 20.5-eV electron energy. A superposition of 96% $d\,^3\Pi_u$ and 4% $e\,^3\Sigma_u^+$ is shown as a solid curve on Fig. 9 and it is seen to follow the data points fairly well. Although the model used for the calculation is an oversimplification, one finds that even a small admixture of direct dissociation gives a dramatic improvement in the fit of the theory to the observed angular distributions.

[46]For energy of dissociation E_0, where $E_0 \gg kT$, the spread in translational energy owing to the thermal motion of the parent H_2 molecule is (Ref. 10) $dN/N = (\frac{1}{2}\pi kTE_0)^{1/2} \times e^{(E^{1/2}-E_0^{1/2})^2}\,dE$. The width at half-maximum is given by $W = [(11/2)kTE_0]^{1/2}$. For $T = 400$ °K and $E_0 = 0.25$ eV, W is equal to 0.218 eV.

[47]The value of σ for 4-eV H(2s) atoms is not known and using 2×10^{-14} cm^2 is an approximation to the actual value. It is noted, however, that the factor $(\sin\theta) \times e^{n\sigma a/\sin\theta}$ is a slowly changing function. A 50% change in σ results in a 10% change in $(\sin\theta)\, e^{n\sigma a/\sin\theta}$.

[48]In order to have sufficient H(2s)-atom intensity, it was necessary to make the electron-gun pulse width 1.5 μsec. This introduces an uncertainty in the kinetic energy of +1.5 and −0.9 eV.

[49]S. Dushman, *Scientific Foundations of Vacuum Technique* (Wiley, New York, 1962).

[50]The known flux was obtained by connecting a gas-filled vessel with an orifice of known size to the source chamber. The density in the vessel was calculated from the ideal-gas law, $n = p/kT$, after the pressure of the vessel was measured directly with a calibrated thermocouple gauge (see Fig. 16). The flux is given by $\frac{1}{4}nvA$.

[51]L. Loeb, *The Kinetic Theory of Gases* (McGraw Hill, New York, 1934), pp. 99–103.

[52]J. C. Zorn, G. R. Carignan, J. C. Pearl, D. P. Donnelly, and J. R. Caldwell, NASA Report No. CR-61320, 1970, Appendix II (unpublished).